International Journal of Geotechnical Earthquake Engineering
Volume 13 • Issue 1

Numerical Modeling of Quaternary Sediment Amplification:

Basin Size, ASCE Site Class, and Fault Location

Rajesh Parla, Indian Institute of Technology, Hyderabad, India*
Surendra Nadh Somala, Indian Institute of Technology, Hyderabad, India

ABSTRACT

The main objective of this study is to understand the dependency of basin amplification on-site and source parameters employing high computational numerical simulations. This study mainly addresses the effect of fault dip, size of the basin, site classification, and position of the basin on wave amplification. Two dip angles are considered, 7 and 9 degrees, in this study to estimate the factor of amplification. Amplifications observed at the basin center and basin edge station for three different sizes of the basin are analyzed. Simulation results obtained from three different models with the ASCE site class C, D, and E basin sediment specifications compared. To analyze the effect of basin relative position on amplification, the authors studied a model with two different basins embedded in bedrock, back and forth of the fault. This study observed multiple peaks at different time periods in response spectra drawn to amplification ratio versus time periods.

KEYWORDS

ASCE site class, basin amplification, numerical simulation, Quaternary sediments, site amplification

INTRODUCTION

Most of the densely populated urban areas are located on or near sediment-filled basins (Mexico, Kathmandu, etc.). The observations of past earthquakes have shown that the ground motions recorded in basins can be affected by many factors such as mechanical properties of sediment materials, faults rupture scenarios, depth, and distance of epicenter from the basin. Even the earthquakes originating at distant epicenters, the urban areas in sedimentary basins experienced long and stronger ground motions due to basin amplification. One of the examples is the 1985 Michoacán Mexico earthquake (Atienza et al., 2016; Rial et al., 1992), where Mexico City, sitting on a basin at a distance more than 350 km from the epicenter, suffered a Mercalli intensity of IX. The basin amplification also increases the duration of ground shaking (Atienza et al., 2016; Kaneko et al., 2018, 2019), which is also observed in this study by numerical simulations. Studies have observed that, the basin amplified ground motion increases the consequences of an earthquake on civil infrastructure (Marafi et al., 2017; Parla et al., 2022; Somala et al., 2022). The basin amplification is largely controlled by stiffness and damping of material, and depth of the sedements (Jakka et al., 2015).

The combined effect of impedance contrast between the basin and surrounding bedrock and wave focusing due to the limited extent of sediments are the main reasons for basin amplification (Semblat

DOI: 10.4018/IJGEE.303589
*Corresponding Author

et al., 2004). The basin effect can be studied by directly investigating ground records or numerical simulations (Frankel & Vidale, 1992; Niu & Dravinski, 2003; Semblat et al., 2011). The availability and exposure of high performance computing resources, the study of seismic source and site effects has emerged in recent years(Chanda et al., 2021; Saha et al., 2022; Veggalam et al., 2021). Along with the impedance contrast, topography also plays a vital role in affecting the amplitude and pattern of basin amplification (Bard & Bouchon, 1985; Niu & Dravinski, 2003). A series of recent studies have indicated that the wave focusing and basin edge effects in sediment basins are also the leading causes of long duration ground shaking (Baher & Davis, 2003; Brissaud et al., 2020; Graves et al., 1998; Kawase, 1996; Stephenson et al., 2000).

Semblat et al. (2002) has used the Boundary element method to analyze the effect of local topography on basin amplification in Caracas (Venezuela) and observed the highest amplification of factor up to 27 at the deepest area of deposits (400m). Liu et al., (2016)) suggested that the basin with soft intermediate layers can exhibit higher amplification (around 80) than the basin with homogeneous sediments (around 20). In this present work, we modeled a 2D bowl-shaped basin with four soft sediment layers embedded in the rock to study the characteristics of basin amplification. Semblat et al. (2005) also observed the influence of local geology on seismic amplification by numerical simulation with the Boundary Element Method. They found a maximum amplification factor of 9.5 at the basin center for vertically incident SH wave with 0.8 Hz frequency. The aspect ratio of width to basin depth also significantly affects seismic amplification. The basin's aspect ratio highly influences the fundamental frequency of the basin, and maximum amplification can be expected for basins with the lowest aspect ratio (Fajardo et al., 2016). We considered three different basin dimensions to address the effect of basin size on maximum amplification factors. Apart from basin materials, the depth of source also influences the scattering of waves inside the basin (Lee et al., 2009). The maximum amplification factor in the basin also depends on the type of earthquakes, such as crustal, megathrust, and deep intra-slab earthquakes (Cipta et al., 2018). On the other hand source mechanism and source parameters also significant in local site amplification (Karthik Reddy et al., 2021; Parla & Somala, 2022). From the numerical study on the Seattle and Tacoma basins, Wirth et al., (2019) found that shallow thrust earthquakes give a higher amplification factor of 5.5 than shallow strike-slip and deep normal earthquakes that observed maximum amplification factors 4.5 and 3, respectively. Geotechnical failures such as liquefaction, are also inevitable in case of basin amplification (Kumar et al., 2013). State of art methods like probabilistic logic tree approach will also help in seismic hazard assessment considering the local site effects (Sitharam & Vipin, 2010).

A major earthquake of Mw 7.8 in Nepal on 25th April 2015 has shown that the long period structures sitting on sediment-filled basins are more vulnerable to collapse. The Kathmandu basin has been observed to resonate at 4-5 sec period and caused significant damage to tall structures (Galetzka et al., 2015). The rupture of the 2015 Nepal earthquake is unilateral with a rupture speed of 3.0 km/s, and the Kathmandu basin exhibited strong amplification at 0.2 Hz frequency (Wei et al., 2018). The seismic waves generated from Nepal 2015 earthquake were also amplified once they entered deep alluvial deposits near the Indo-Nepal border. The cities in the Indo-Gangetic basin (Sharma et al., 2017) also suffered significant ground motion, stressing the importance of the study of basin amplification both forth and back of ruptured fault. The poor quality of construction, type of structures, and materials used for buildings in the Kathmandu basin further amplified the destruction of the 2015 Nepal earthquake (Adhikari & Ayala, 2020; Whitney & Agrawal, 2017). The studies of past earthquakes in the Kathmandu region often state that the valley's damages were amplified due to site effects (Dixit et al., 2000; Paudyal et al., 2012).

The present study uses the numerical model inspired by the Kathmandu basin and the 2015 Nepal earthquake. The basin amplification and effect of basin size, dip angle, sediment properties, and basin location are addressed using simulated ground motions. Three different basin sizes are considered to study the size effect. Though the source parameters include strike, rake, and dip angle, our present study is limited to addressing the effect of dip angle alone on basin amplification. As the Himalayan faults are predominantly dipping faults with smaller dip angles, we considered 7^0 and 9^0 dip angles to mimic fault systems in that region. The reference model inspired by the Kathmandu basin is compared with three other basin models with ASCE site-class C, D, and E materials to address basin materials effect on the amplification factor. The methodology section describes the finite element scheme and the finite fault source we used in the simulations. PyLith software (Aagaard et al., 2009) has been used to simulate synthetic ground motions. The spectral ratio of simulated and real earthquake data are compared for validation of numerical simulations. The amplification factor is quantified as the ratio of Fourier amplitude of velocity in the basin to Fourier amplitude of velocity at the bedrock station. The bedrock station is located outside the basin. The variation in amplification factors over the time period for different basin-bedrock models are compared in the results and discussion sections. The key insights from the results are summarized in the conclusion section.

MODELLING AND NUMERICAL SIMULATION

The 2D model consists of two major domains, the rock part, and the basin embedded in the rock, as shown in Figure 1. The size of the whole domain is 350 km length and 70.5 km depth; the size of the basin considered in the study is 30.8 km length with a maximum depth of 1.5 km. The basin has 4 sediment layers and rock parts having a total of 8 layers. The velocity model for the rock and basin parts (Galetzka et al., 2015; Paudyal et al., 2012; Wei et al., 2018) used in this study is shown in Table 1. The basin and bedrock parts are discretized with mesh elements of 50 m and 200 m, respectively. PyLith 2.2.1 (Aagaard et al., 2009) is used for numerical simulation with a stable time step of 0.004sec. The maximum resolving frequency of the model with the given mesh size and materials is 1 Hz. The rupture parameters (slip, rise time, and slip time) of the 2015 Nepal earthquake (Avouac et al., 2015) have been used to model line finite fault source. The finite fault is 115 km long with a dip 7^0 to mimic Himalayan faults, primarily low dip converging faults. The rupture initiation point on fault is denoted by the red star on the fault line. Except for the top surface of the domain, all three faces are provided with AbsorbingDampers boundary conditions to prevent seismic wave reflections off the boundaries. This AbsorbingDampers boundary condition, which is simpler than a perfectly matched layer (PML), can perfectly absorb normally incident dilatational and shear waves. We considered two basin stations

Figure 1. 2D model with basin embedded in a rocky stratum. The location of three stations are denoted by inverted triangles.

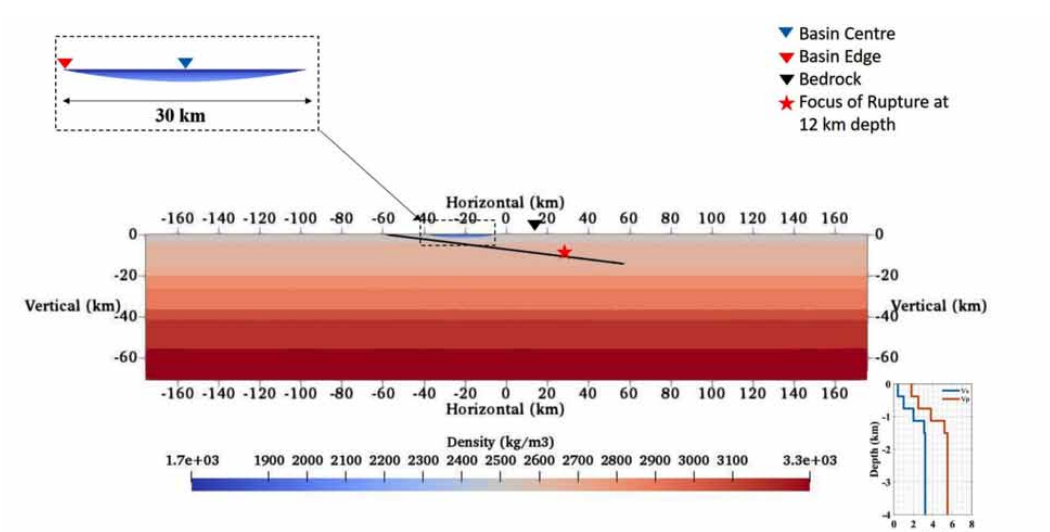

Table 1. 1D Velocity structure for Basin and Bedrock.

	Dimensions (km)	No. of Layers	Thickness of Layers (m)	ρ (kg / m³)	Vs (m/s)	Vp (m/s)	Mesh Size (m)
Basin	30.8 x 1.5	4	375	900 1200 1500 2100	400 1000 2000 3100	1800 2500 3800 5200	50
Rock	350 x 70	8	4000 12000 4000 6500 10000 5000 14000 15000	2530 2640 2690 2830 2900 3070 3170 3300	3200 3400 3500 3700 3850 4150 4200 4300	5500 5850 6000 6450 6650 7200 7500 7900	200

to study the basin amplification at basin center and another at the basin edge. One bedrock station outside the basin at 10 km from the right edge of the basin is also considered as shown in Figure 1.

The 2D model mimicking the Kathmandu basin and 2015 Nepal earthquake is validated by comparing the spectral ratios of real earthquake ground motion and simulated ground motion. The spectral ratio is calculated from Eq (1) (Delgado et al., 2000)

$$\text{Spectral ratio(H/V)}=\sqrt{\frac{Fn^2+Fe^2}{2Fv^2}} \tag{1}$$

where Fn, Fe, and Fv are the Fourier amplitude spectra in North-South (NS), East-West (EW) and vertical directions.

The ground motion records of the Nepal 2015 earthquake at station KATNP (27.7120 N 85.3160 E) located at the basin center (Figure 2) are used to calculate spectral ratio and compared with simulated records as shown in Figure 3. For the 2D model, the spectral ratio is calculated by taking the ratio of Fourier amplitude spectra of horizontal to vertical. It can be observed from Figure 3 that the multiple peaks in amplification are due to basin resonance (Galetzka et al., 2015) and the period where the peaks occurring for 2D simulation are following those of real earthquake. The basin-bedrock model is limited to 1D velocity because of the unavailability of the 3D velocity model of the Kathmandu region. Even with 1D velocity and without topography, the simulated basin-bedrock model seems to match the spectral ratio trend with the real earthquake.

METHODOLOGY

The flowchart highlighting the steps involved in modeling and simulation of 2D basin-bedrock is shown in Figure 4. CUBIT has used for modeling and meshing. The meshed model is exported as .exo file, which is PyLith readable. We have used PyLith software, a Finite Element Method (FEM) based parallel processing tool (Aagaard et al., 2009) for numerical simulations. The source of earthquake is a line finite fault. The elements on the fault are replaced by zero volume cohesive elements, which have additional degrees of freedom in terms of Lagrange multipliers (Aagaard et al., 2009). The rupture parameters slip, slip time, and rise time are shown in Figure 5.

We introduced numerical damping via an artificial viscosity to reduce the high-frequency oscillations that are not accurately resolved by the discretization (Day & Graves, 2002; Knopoff &

Figure 2. Records of ground accelerations during 2015 Nepal earthquake (a) in time scale and (b) in frequency scale.

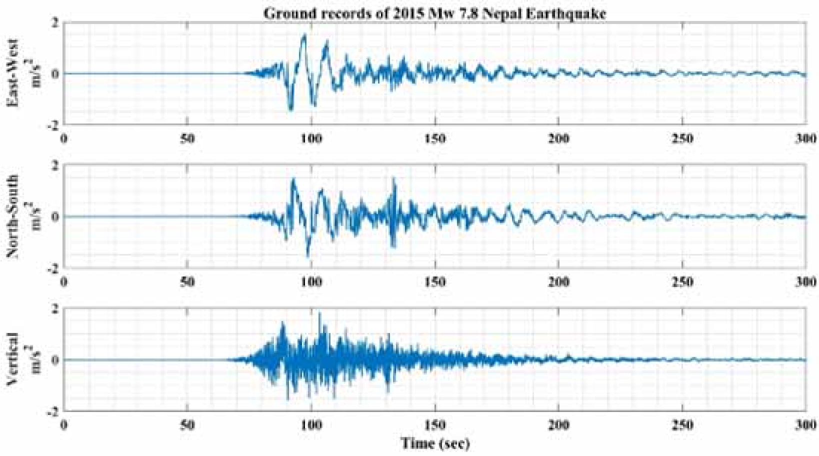

(a)

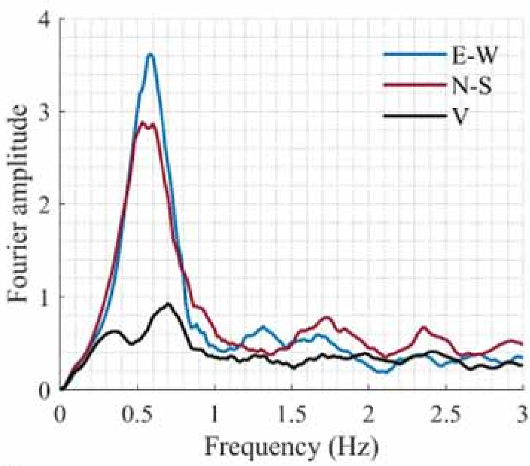

(b)

Figure 3. Comparison of spectral ratio of simulated ground motion with 2015 Nepal earthquake.

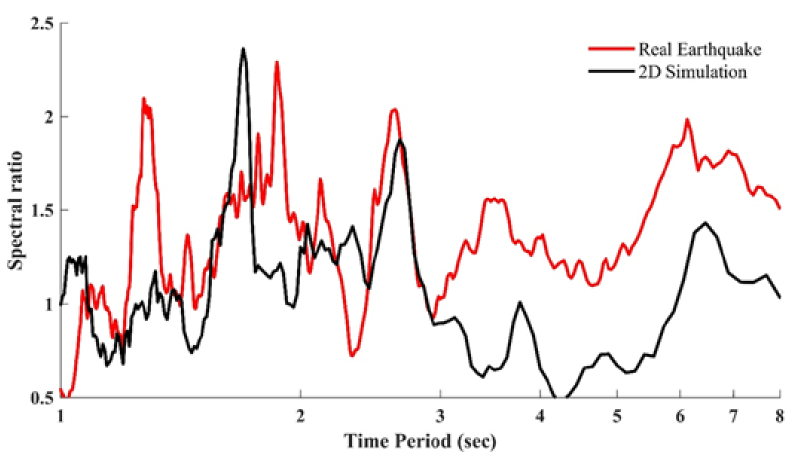

Figure 4. Flowchart of steps involved in modeling and simulations.

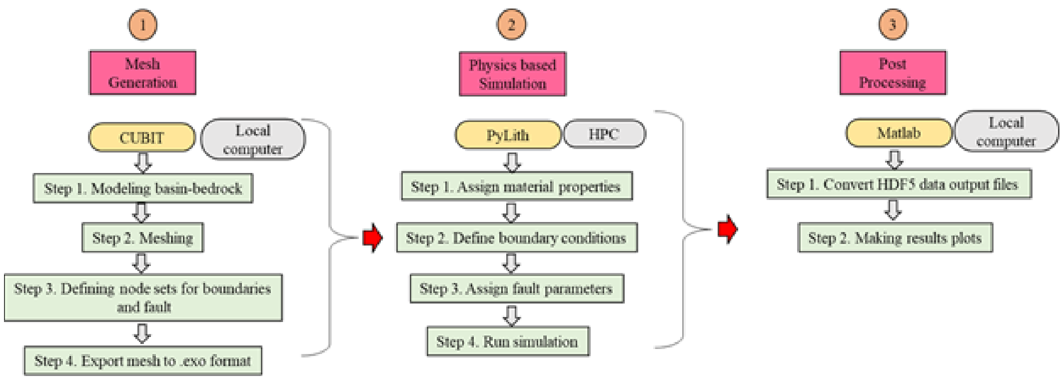

Figure 5. Rupture parameters of fault.

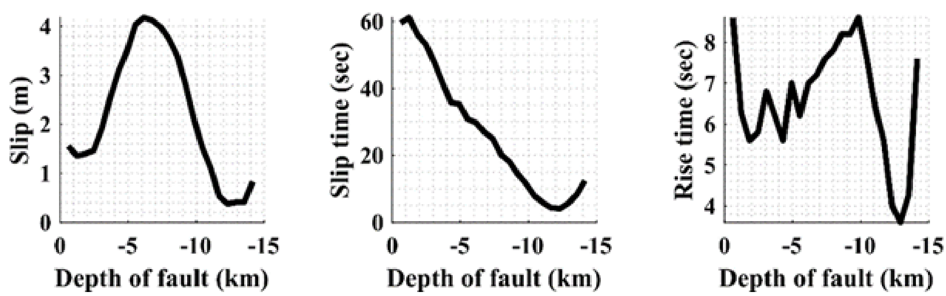

Ni, 2001). Liu-Cosine slip time function (Liu et al., 2016) is used to describe rupture propagation on a finite fault line with rise time varying between 0.6 sec to 8.6 sec. As the meshing is done using triangular elements, FIATSimplex (finite element automatic tabulator) quadrature scheme and basis functions are used. The field variable (in this case displacement) is considered to be varying linearly within the element. The maximum resolvable frequency of the 2D model is 1 Hz. The long period structures (4-5 sec) like Dharahara tower were the most affected during the 2015 Nepal earthquake (Avouac et al., 2015). Since our interest is to study the Kathmandu-like basin effects, the resolved frequency (1 Hz) is sufficient (Jayalakshmi et al., 2019; Lee et al., 2008; Narayan, 2005). The amplification factors presented in this study are defined as the ratio of Fourier amplitudes of velocity in the basin to the Fourier amplitudes of velocity recorded at bedrock stations as shown in Eq.(2).

$$AF = \frac{FV_b}{FV_r} \tag{2}$$

where AF is amplification factor, V_b is the ground velocity at basin center, and V_r is the ground velocity at bedrock station.

The spatial database for material, fault parameters, and boundary conditions are provided in the form of SimpleDB (a kind of spatial database) to the node sets created during the meshing of the model. The basin will exhibit a maximum spectral amplification at its resonant frequency. The one-dimensional resonant frequency of the sediment basin can calculate from Eq.3 (Kramer, 1996)

$$f_c = \frac{V_s}{4\text{H}} \tag{3}$$

where *Vs* is shear wave velocity in sediment basin, H is the thickness of sediment layer.

For multi-layered sediment basins with n layers, the resonant frequency can be expressed as in Eq (4) by considering a single equivalent layer (Paudyal et al., 2012).

$$f_c = \frac{\sum_{i=1}^{n} V_{si} H_i}{4\left(\sum_{i=1}^{n} V_{si} H_i\right)^2} \tag{4}$$

For the 1D velocity profile of the basin we considered in this study (Table.1), the resonant frequency of the basin from Eq. (4) will be 0.27 Hz or 3.7 sec period.

RESULTS AND DISCUSSION

Effect of Dip Angle

The source dependence of basin amplification is an important factor in the seismic hazard assessment for urban areas in basins. Apart from source location and depth of source, the rupture mechanism also has a significant effect on basin amplification (Wirth et al., 2019). In this section, the effect of dip angle on basin amplification is studied by two basin-bedrock models with 7^0 and 9^0 dip angles. The simulated ground velocity records at basin center, basin edge, and bedrock stations are shown in Figure 6. It can be observed that the ground velocities recorded at basin center and basin edge are having higher values compared to bedrock station for both the dip angles. The results shown in Figure 7 demonstrated that the change in dip angle will significantly affect the amplification factors. The basin edge station recorded higher amplification factors compared to basin center for both 7^0 and 9^0 dip angles.

The vertical component of ground motion exhibits higher AF at a lower time period from dip angles. The AF is recorded at the basin edge with a value of 11 for both models. Galetzka et al. 2015 observed multiple peaks in amplification for the east component (horizontal in our 2D model) of ground motion at basin stations KATNP and NAST between 1 -10 sec. Our 2D model with dip

Figure 6. Ground velocity record in the basin and at bedrock station for 7^0 and 9^0 dip fault.

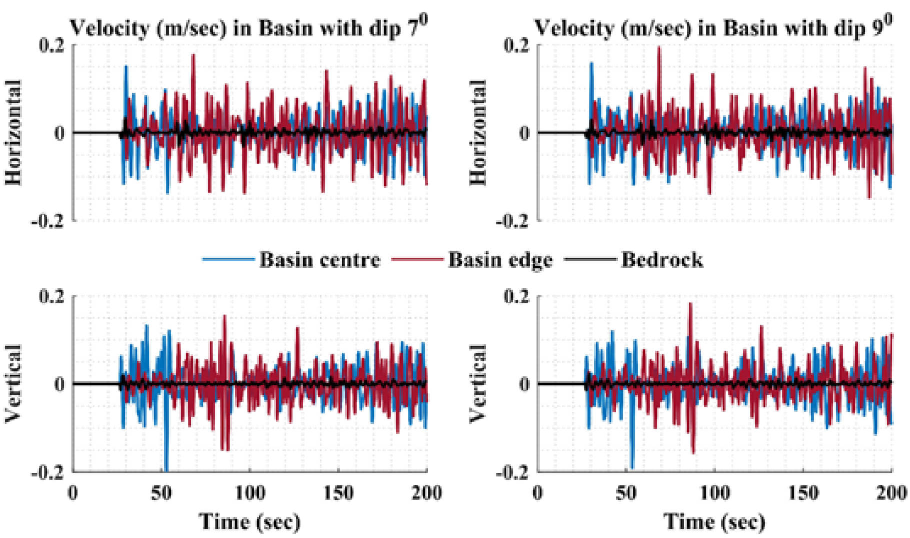

Figure 7. Amplification factors for dip angles 7^0 and 9^0

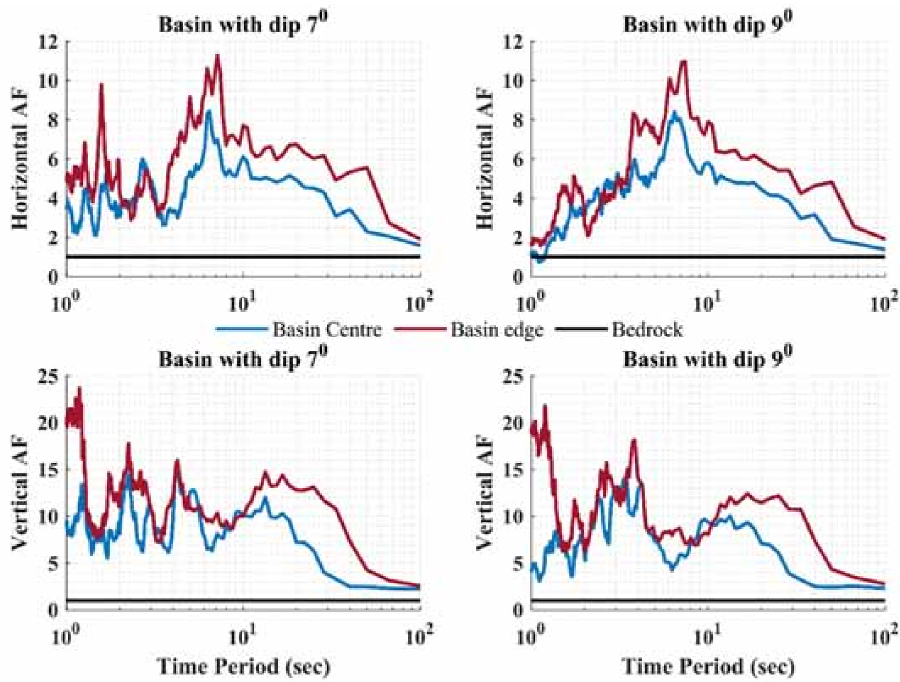

$7^{0,}$ which mimics the Kathmandu basin and Nepal 2015 earthquake, also exhibits multiple peaks in amplifying horizontal components at basin center and basin edges between 1-10 sec. It is also clear that the model with 9^0 has no multiple peaks in AF for the horizontal component. The multiple peaks in amplification at different time periods are due to basin resonance. The trend in AF shown in Figure 5 depicts the occurrence of multiple peaks in AF due to basin resonance depending on the combined effect of basin materials and dip angle. The maximum value of amplification factors is shown in Figure 8, which depicts the amplification is more at the basin center than at the basin

Figure 8. Maximum Amplification factors for dip angles 7^0 and 9^0

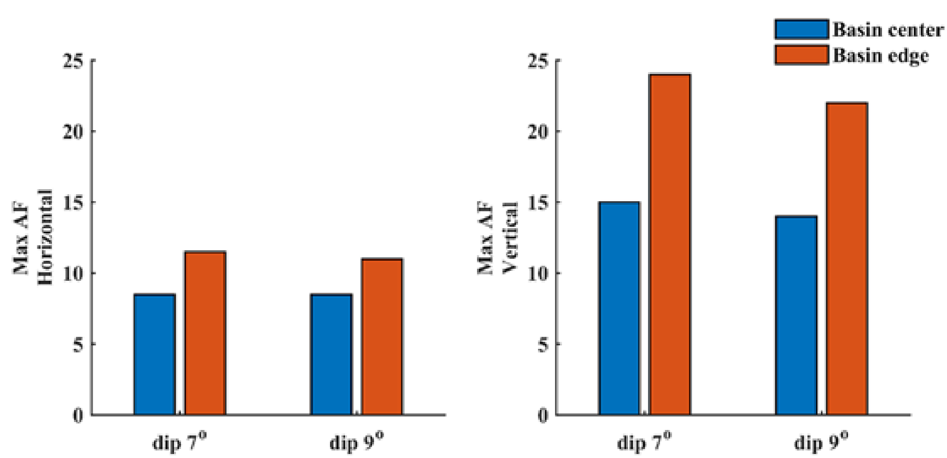

edge. The main reason for this could be that sediment thickness is more at the basin center. It is also observed that the difference in maximum amplification factors between basin center and basin edge is more for the vertical component.

Effect of Size of the Basin

Studies showed that there is a correlation between basin depth and amplification factors (Choi et al., 2005; Day et al., 2008; Field, 2000; Semblat et al., 2002, 2005), and observations suggested that maximum amplification can occur above the thickest sediment layers (e.g., Graves et al. 1998; Chen 2003; Cipta et al. 2018). In general, most researchers use depth to 1.5 km/s or 2.5 km/s isosurfaces to examine the effect of basin depth on wave amplification (e.g., Campbell 1997; Lee and Anderson 2000; Steidl 2000; Day et al. 2008). But the basin amplification is site-specific (Ivanovic & Sanja, n.d.; Mascandola et al., 2017; Nozu et al., 2006; Weatherill et al., 2020; Wirth et al., 2019), and the geometry of sediment layers also affects the magnitude of amplification factors and the period where the peak amplification can occur (Semblat et al., 2004, 2005). We modeled three basins with different basin dimensions, as shown in Table.2, to study the effect of basin size on amplification factors. All three basins consist of 4 sediment layers with different Vs and Vp to incorporate the effect of sediment layering on basin amplification and the effect of basin size. Since the finite fault can produce complete waveforms, it better represents earthquakes than the point and plane wave sources.

In Figure 9, the ground velocities recorded at the basin center, basin edge, and bedrock station reveal that the basin size plays a considerable role in affecting the velocity amplitudes of ground motion. The velocity-time histories recorded at the basin center and basin edge are distinct for the three different basin sizes. It can be further observed that Basin-A with the highest aspect ratio (width/depth) has higher velocity amplitudes at the basin center than the basin edge. The amplification factors calculated from synthetic ground motion for the three basins (A, B, and C) are compared with empirical models of Day et al. (2006, 2008), as shown in Figure 10. The empirical models have considered depth to 1.5 km/s isosurfaces to represent the basin depth. In our 2D model, the average shear wave velocity over the four strata is 1.625 km/s. The amplification factors at a longer period (8 s) for the 2D model are very close to the mean of amplification factors obtained from empirical models. For the 2 sec and 4 sec periods, amplification factors from 2D simulations are within the range of +sigma and –sigma of empirical models.

Figure 11 and Figure 12 show the variation in amplification factors with time period for three basins. The maximum horizontal amplification factor at basin centers in Basin A, B, and C, as shown in Figure 13, are 12, 8, and 7, and at the basin edge are 5, 11, and 6, respectively. The maximum vertical amplification factors at basin centers in Basin A, B, and C are 20, 15, and 15 and at basin edge 15, 24, and 9. It is observed that the maximum amplification factor is dominant at the basin center for the smallest basin. The maximum amplification factor is dominant at the basin edge for the other two basins. The predominant edge reflections and multiple converging of reflected waves at basin edge could be the main reason for the higher amplification at basin edge for two basins.

Effect of Site Class

The material properties of sediments in the basin or the site classes have a potential role in affecting the wave amplification in the basins. The amplification of ground motion is site-specific and material properties influence the degree of ground motion amplification. To understand the effect of material properties of the sediments in the basin on wave amplification, we considered three different velocity models with ASCE site class C, D and E and the velocity model mentioned in table 1.

The basin dimensions and fault parameters are identical for all four models and the simulation results are presented as ground velocities and amplification factors. The basin model with ASCE site class E has the lowest shear wave and P wave velocities and lowest density compared to the rest of the three basin models. The ground records shown in Figure 14 are with different amplitude values depending on the site class of the basin model. The ground velocities at basin edges have

Table 2. Dimensions of three different size basins.

Basin name	Width (km)	Depth (km)	Aspect ratio (Width / Depth)
Basin A	25	1	25
Basin B	30.8	1.5	20.5
Basin C	40	2.5	16

Figure 9. Ground velocity record in basin A, basin B, basin C and at bedrock station.

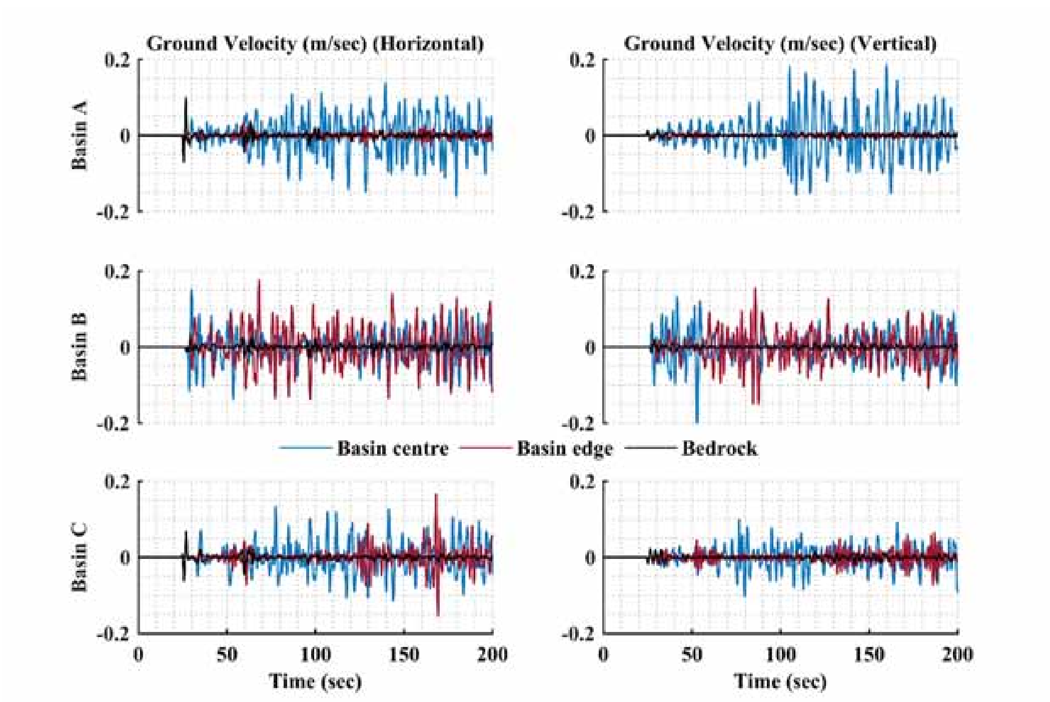

Figure 10. Comparing amplification factors of simulated ground motions with Day et al. (2006, 2008) empirical models.

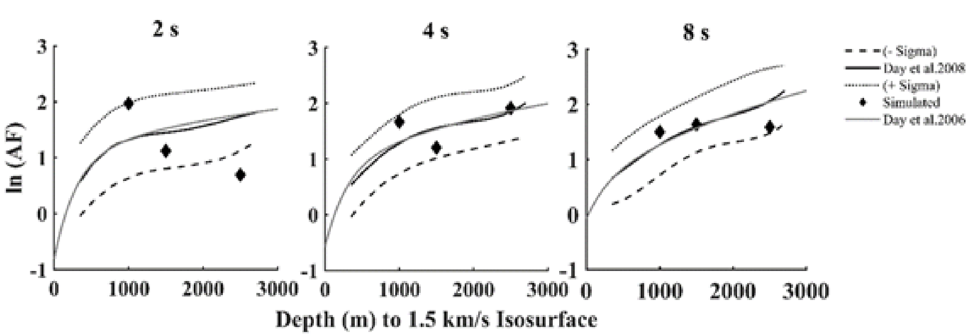

Figure 11. Horizontal amplification factors at basin center, basin edge, and bedrock stations for three basins with different sizes.

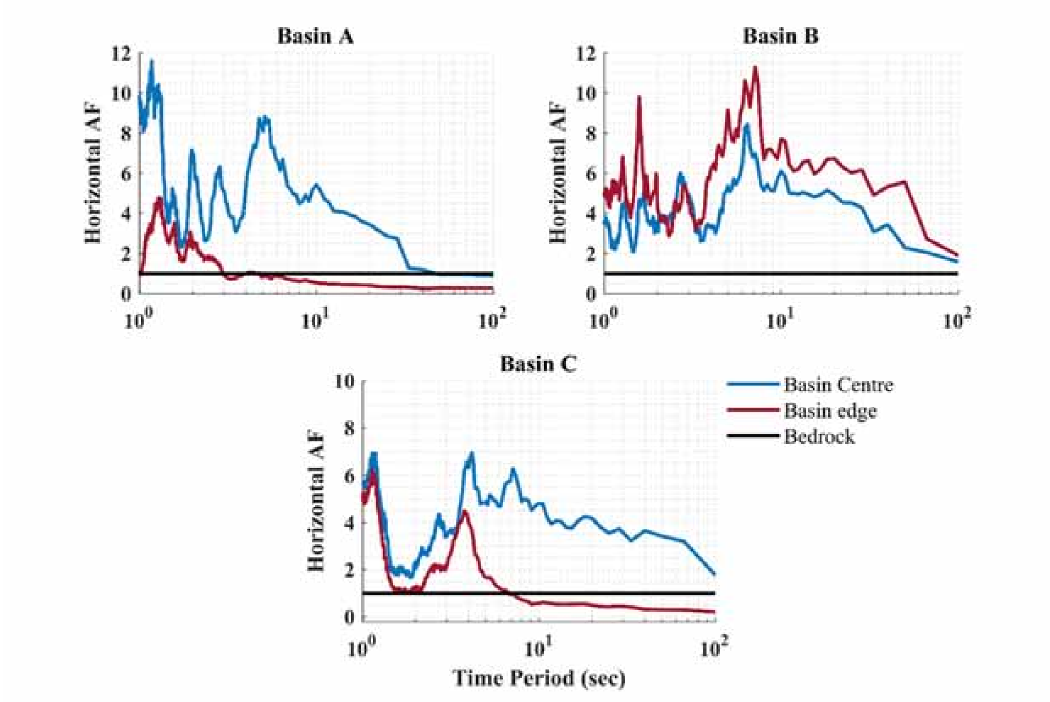

Figure 12. Vertical amplification factors at basin center, basin edge, and bedrock stations for three basins with different sizes.

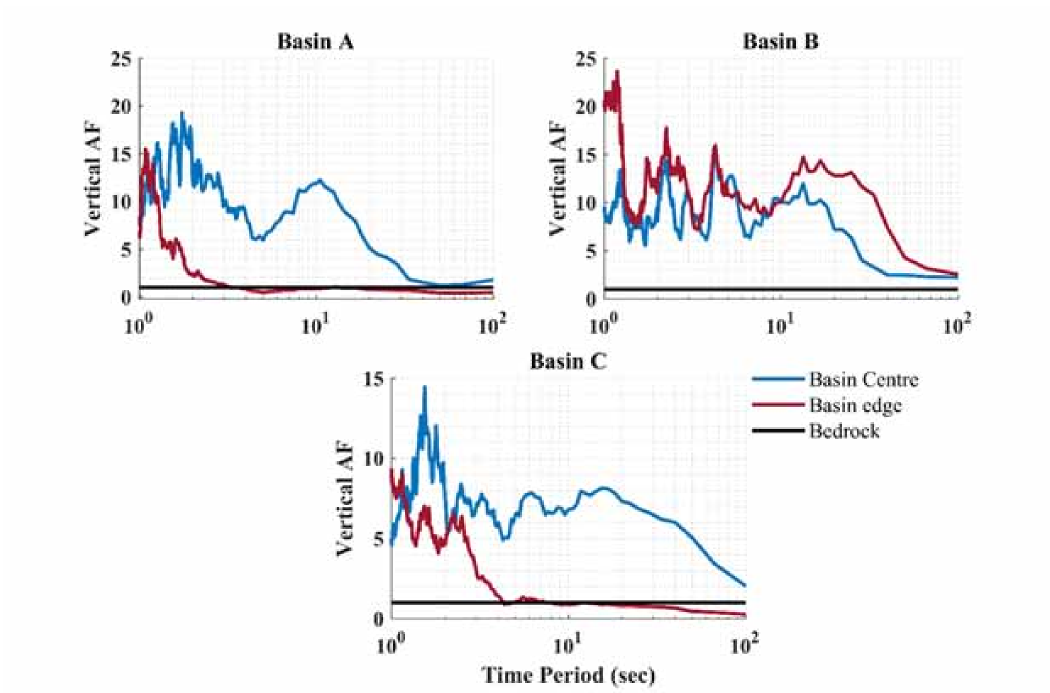

Figure 13. Maximum Amplification factors for three basins with different sizes.

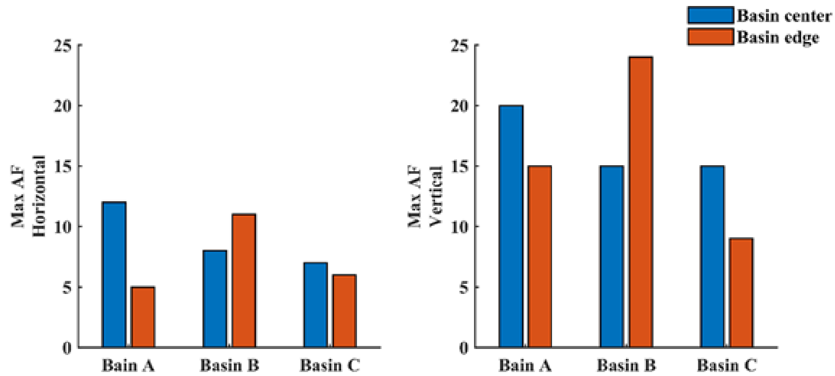

Figure 14. Ground velocity recorded in basins with ASCE site class C, D, E and at bedrock station.

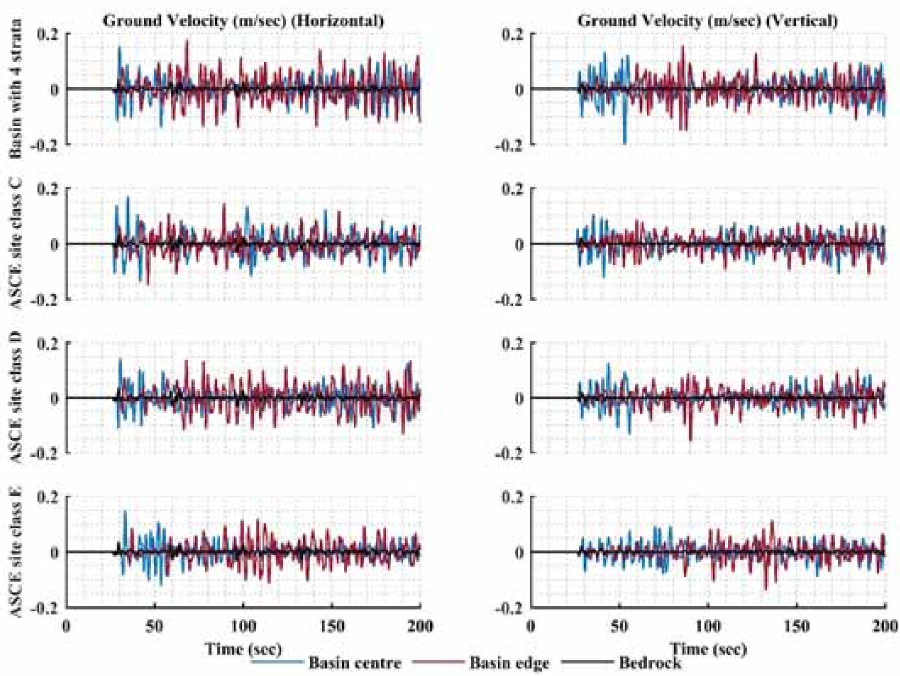

Table 3. Specifications of basins with different site classes.

Basin type	Width (km)	Depth (km)	No. of Layers	ρ (kg / m³)	Vs (m/s)	Vp (m/s)
Basin with 4 Strata	30.8	1.5	4	900 1200 1500 2100	400 1000 20003100	1800 2500 38005200
ASCE site class – C	30.8	1.5	1	1670	500	850
ASCE site class – D	30.8	1.5	1	1230	250	425
ASCE site class - E	30.8	1.5	1	1080	150	255

higher amplitudes due to edge reflections. The amplification at different time periods are shown in Figure 15 and Figure 16 for all the basin models. The model with four alluvial strata experienced higher amplification factors at basin center and basin edge than the three considered ASCE site class models due to impedance contrast between the multiple layers in the basin. A decreasing trend in peak amplification factors for vertical component for different basins can be observed.

Figure 15. Horizontal amplification factors at basin center, basin edge and bedrock stations for basins with ASCE site class C, D and E.

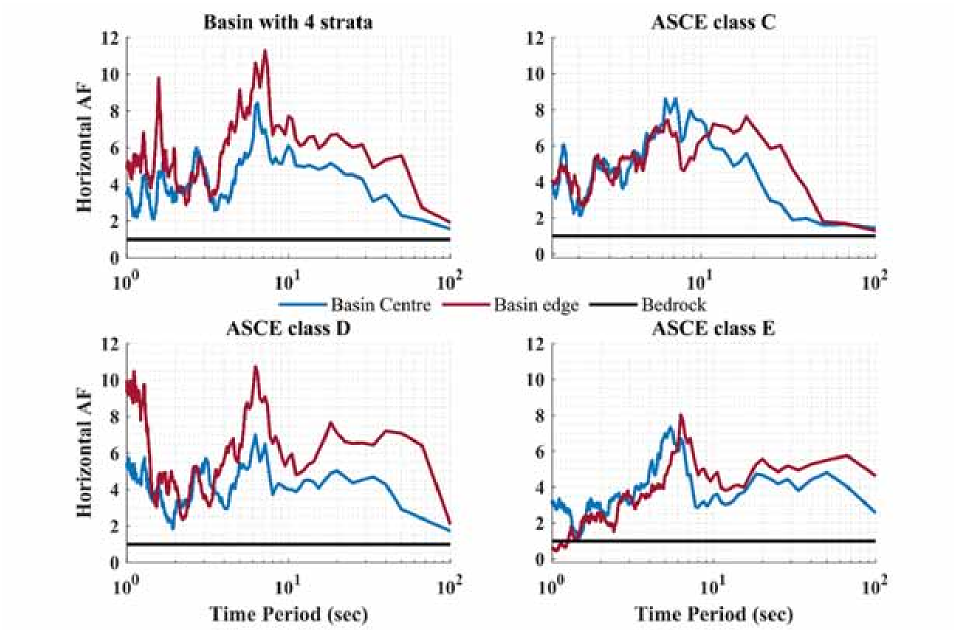

Figure 16. Vertical amplification factors at basin center, basin edge and bedrock stations for basins with ASCE site class C, D and E.

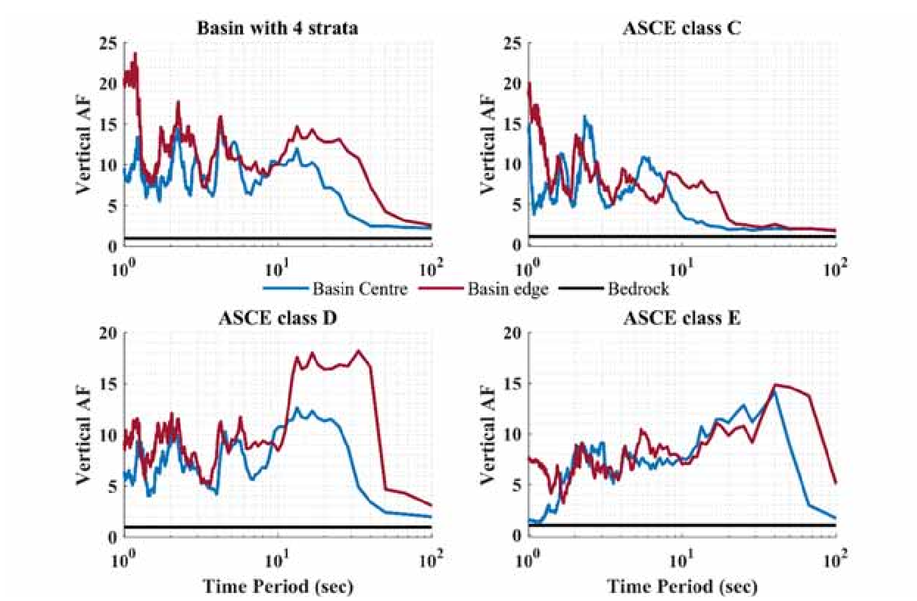

Figure 17. Maximum amplification factors at basin center and basin for basins with ASCE site class C, D and E.

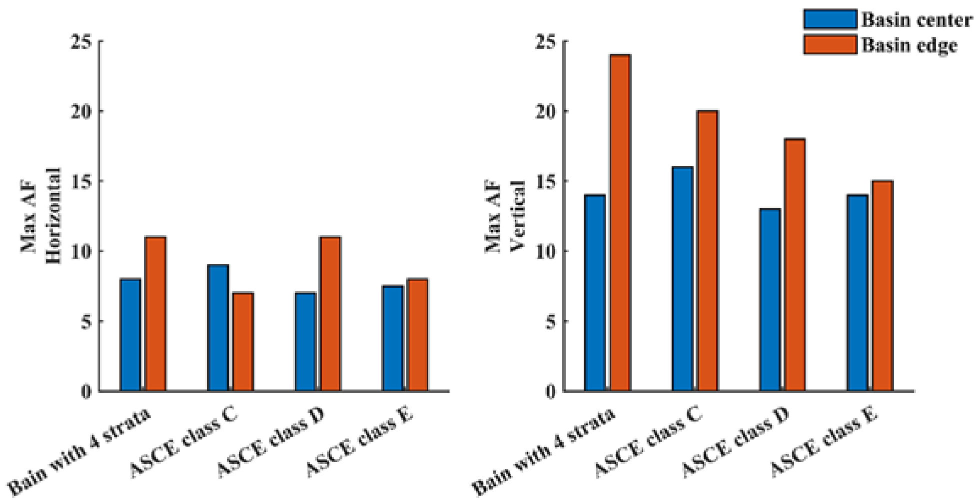

Effect of Basin Location

The basin's location with respect to the rupture direction also has a great effect on basin amplification. A secondary basin was introduced in the model at back of fault to study the effect of wave amplification behind the ruptured fault. The finite element model consisting of two basins embedded in the rock strata are shown in the Figure 18. The secondary basin has been given a name Basin-G and the basin is located above the fault as Basin-K to mimic Indo-Gangetic basins and Kathmandu. The considered model is simulated with a finite fault line as source and the material in Basin-G has a velocity model as given in Table4. The material properties of Basin-K and rock are the same as mentioned in

Figure 18. 2D model with basins in front and behind the fault.

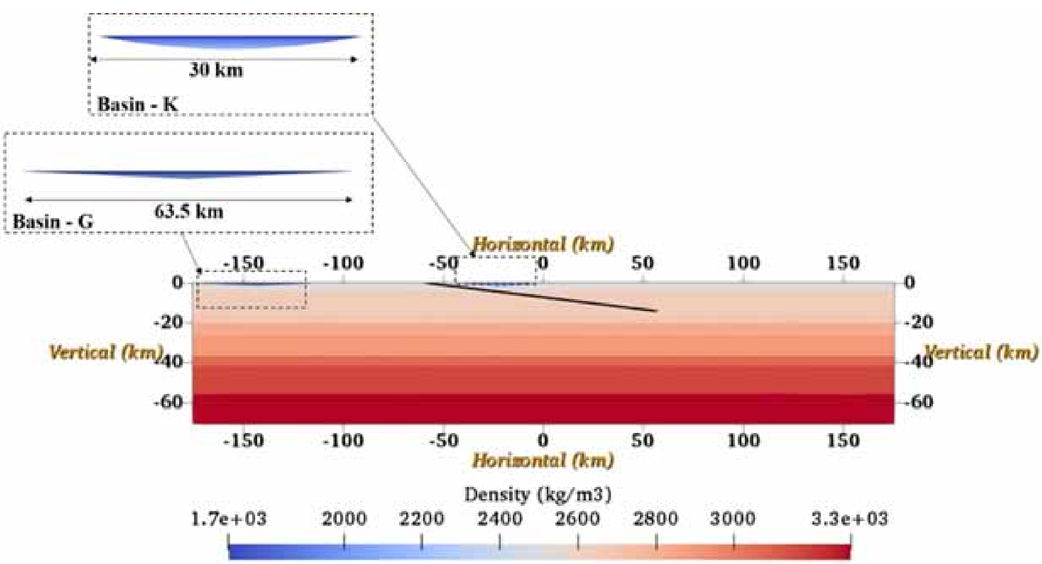

Table 4. Velocity structure of Basin-G.

Dimensions (km)	No. of Layers	Thickness of Layers (m)	ρ (kg / m³)	Vs (m/s)	Vp (m/s)	Mesh Size (m)
Width = 63.5 Depth = 0.15	4	375	1700 1900 2000 2100	380 890 1300 1800	1500 1750 1850 2000	50

Table1. The simulations have been done for two fault dip angles 7^0 and $9^{0,}$ and the ground velocities are recorded at basin center, basin edge and bedrock station in Figure 19. The spectral variation in amplification factor is shown in Figure 20, which reveals the basins in the region behind the active faults also having equal threats of basin amplification. A de-amplification is observed at basin edge station in Basin-G for both the dip angles at some time periods. Since the source is far from the basin, the effect of edge induced reflection and multiple interactions at edge is minimal in this case. It is also observed that the time period where peak amplification occurring in basin is longer for the basin far from source compared to the basin resting directly above the fault. Figure 21 shows the maximum amplification of 6 for horizontal and 10 for vertical components in Basin-G.

Figure 19. Ground velocity recorded in Basin-G and with 7^0 and 9^0 dip fault.

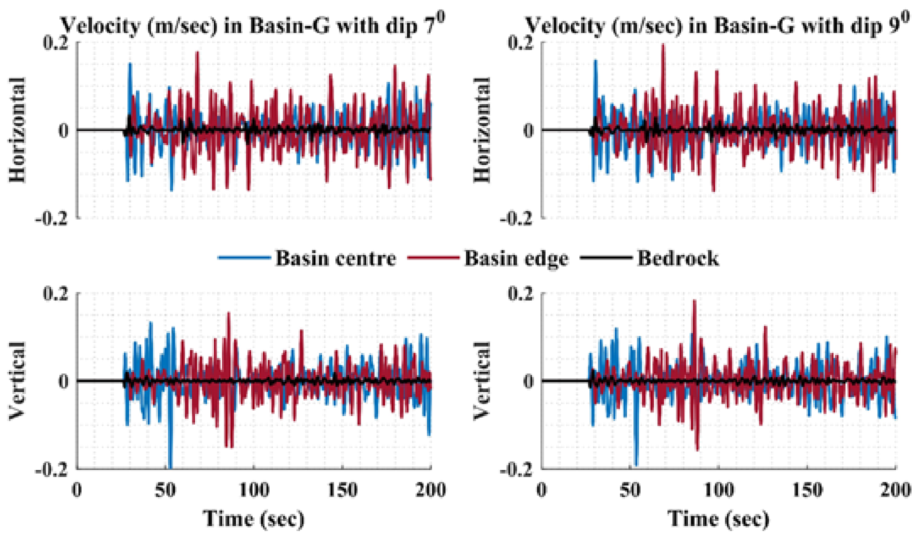

CONCLUSION

The main focus of the work described in this research article is to give an insight to the dependency of basin amplification on some of the fault and site parameters such as dip angle, basin size, material properties, and basin position. We took advantage of the availability of the finite fault data of the 2015 Gorkha earthquake and sediment properties of Kathmandu valley to set up base simulations and carry out a parametric study as we intended. The principal findings are summarized as follows:

Figure 20. Ground motion amplification observed in Basin-G at basin station 2 and basin station 3 for two dip angles 7⁰ and 9⁰.

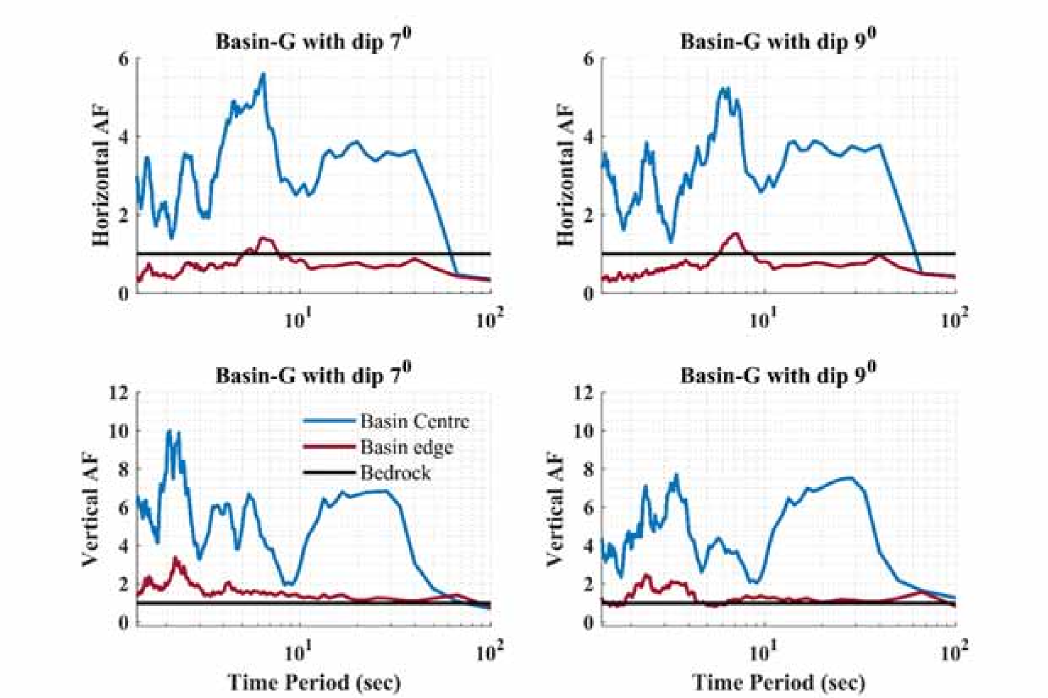

Figure 21. Maximum amplification factors at basin center and basin edge in Basin-G.

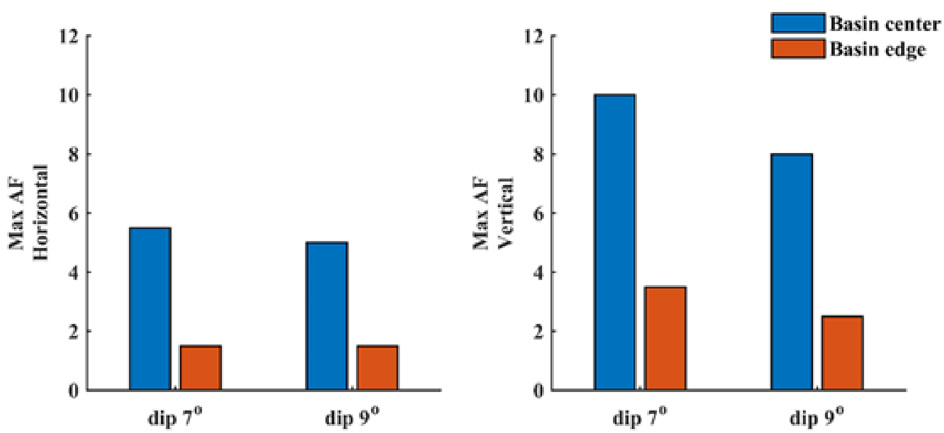

- The multiple rises in amplification at different time periods are associated with basin resonance, and the structural response can also be affected by this basin resonance. In hazard assessment for an event that erupted in the sediment basins, the basin resonance carries an important role in risk and loss estimation.
- The study on the effect of basin size inferred that the largest basin may or may not be experienced the highest amplification if the fault is very nearer to the basin. The fundamental frequency of the basin plays a vital role in basin amplification. For the basins with fundamental frequency nearly matching with the frequency of incident waves, the amplification will be more. Since the

fundamental frequency is a function of material and geometry, a study of wide range of basin shapes and sizes is significant.

- It is observed that three ASCE site class models exhibit comparatively less amplification than the model with multiple layers. The reason is the impedance contrast between the multiple soil layers. The multiple impedance contrasts with in the basin, allows the waves to under go multiple reflections and refractions while passing across the depth of basin.
- For the configurations where edge induces waves and their interaction is dominant, high amplifications are observed at basin edges.
- For the basins located right above the fault line, the amplification factors observed at the basin edge are predominantly higher than at the basin center. This may be associated with the multiple interactions between edge-induced waves at basin edge and lead to more seismic wave amplification.
- On the other hand, it is observed that in the model embedded with Basin-G, which is far from the fault line, the peak amplification of waves is mainly observed at the basin center where sediment depth is maximum. This concludes that maximum amplification happens at the basin center for far-field ground motion, and for near-field, maximum amplification occurs at the basin edges.

FUNDING AGENCY

This research received no specific grant from any funding body in the public, commercial, or not-for-profit sectors.

ACKNOWLDGMENTS

Funding from MoES/P.O(Seismo)/1(304)/2016 is greatly acknowledged.

CONFLICTS OF INTEREST

We wish to confirm that there are no known conflicts of interest associated with this publication and there has been no significant financial support for this work that could have influenced its outcome.

PROCESS DATES:

Received: June 22, 2021, Revision: April 27, 2022, Accepted: April 28, 2022

CORRESPONDING AUTHOR:

Correspondence should be addressed to Rajesh Parla; ce18resch11006@iith.ac.in

REFERENCES

Aagaard, B., Kientz, S., Knepley, M., Somala, S., Strand, L., & Williams, C. (2009). PyLith User Manual, (Version 1.5.0). Pasadena, CA.

Adhikari, R. K., & Ayala, D. (2020). 2015 Nepal earthquake: Seismic performance and post-earthquake reconstruction of stone in mud mortar masonry buildings. *Bulletin of Earthquake Engineering*, *18*(8), 3863–3896. doi:10.1007/s10518-020-00834-y

Atienza, V. M., Tago, J., Sanabria-Gómez, J. D., Chaljub, E., Etienne, V., Virieux, J., & Quintanar, L. (2016). Long Duration of Ground Motion in the Paradigmatic Valley of Mexico. *Scientific Reports*, *6*(1), 1–9. doi:10.1038/srep38807 PMID:28442746

Avouac, J.-P., Meng, L., Wei, S., Wang, T., & Ampuero, J.-P. (2015). Lower edge of locked Main Himalayan Thrust unzipped by the 2015 Gorkha earthquake. *Nature Geoscience*, *8*(9), 708–711. doi:10.1038/ngeo2518

Baher, S. A., & Davis, P. M. (2003). An application of seismic tomography to basin focusing of seismic waves and Northridge earthquake damage. *Journal of Geophysical Research. Solid Earth*, *108*(B2). Advance online publication. doi:10.1029/2001JB001610

Bard, P. Y., & Bouchon, M. (1985). The two-dimensional resonance of sediment-filled valleys. *Bulletin of the Seismological Society of America*, *75*(2), 519–541. doi:10.1785/BSSA0750020519

Brissaud, Q., Bowden, D. C., & Tsai, V. C. (2020). Extension of the Basin Rayleigh-Wave Amplification Theory to Include Basin-Edge Effects. *Bulletin of the Seismological Society of America*, *110*(3), 1305–1322. doi:10.1785/0120190161

Campbell, K. W. (1997). Empirical Near-Source Attenuation Relationships for Horizontal and Vertical Components of Peak Ground Acceleration, Peak Ground Velocity, and Pseudo-Absolute Acceleration Response Spectra. *Seismological Research Letters*, *68*(1), 154–179. doi:10.1785/gssrl.68.1.154

Chanda, S., Raghucharan, M. C., Karthik Reddy, K. S. K., Chaudhari, V., & Somala, S. N. (2021). Duration prediction of Chilean strong motion data using machine learning. *Journal of South American Earth Sciences*, *109*, 103253. doi:10.1016/j.jsames.2021.103253

Chen, K. C. (2003). Strong ground motion and damage in the Taipei basin from the Moho reflected seismic waves during the March 31, 2002, Hualien, Taiwan earthquake. *Geophysical Research Letters*, *30*(11), 1551. doi:10.1029/2003GL017193

Choi, Y., Stewart, J. P., & Graves, R. W. (2005). Empirical Model for Basin Effects Accounts for Basin Depth and Source Location. *Bulletin of the Seismological Society of America*, *95*(4), 1412–1427. doi:10.1785/0120040208

Cipta, A., Cummins, P., Irsyam, M., & Hidayati, S. (2018). Basin Resonance and Seismic Hazard in Jakarta, Indonesia. *Geosciences*, *8*(4), 128. doi:10.3390/geosciences8040128

Day, G., & Graves, E. (2002). Effect of a shallow weak zone on fault rupture: Numerical simulation of scale-model experiments. *Bull. Seismol. Soc. Am., 92*(8*),* : 10.1785/0120010273

Day, G., Graves, R., Bielak, J., Dreger, D., Larsen, S., Olsen, K. B., Pitarka, A., & Ramirez-Guzman, L. (2008). Model for Basin Effects on Long-Period Response Spectra in Southern California. *Earthquake Spectra*, *24*(1), 257–277. doi:10.1193/1.2857545

Day, S., Bielak, J., Dreger, D., Graves, R., Larsen, S., Olsen, K., Pitarka, A., & Ramirez-Guzman, L. (2006). *Numerical simulation of basin effects on long-period ground motion*.

Delgado, J., López Casado, C., Giner, J., Estévez, A., Cuenca, A., & Molina, S. (2000). Microtremors as a Geophysical Exploration Tool: Applications and Limitations. *Pure and Applied Geophysics*, *157*(9), 1445–1462. doi:10.1007/PL00001128

Dixit, A. M., Dwelley-Samant, L., Nakarmi, M., Pradhanang, S., & Tucker, B. (2000, January 1). The Kathmandu Valley Earthquake Risk Management Project. *Evaluation*. doi:10.13140/2.1.4625.0244

Fajardo, K. C. M., Semblat, J.-F., Chaillat, S., & Lenti, L. (2016). Seismic Wave Amplification in 3D Alluvial Basins: 3D/1D Amplification Ratios from Fast Multipole BEM Simulations. *Bulletin of the Seismological Society of America*, *106*(3), 1267–1281. doi:10.1785/0120150159

Field, E. H. (2000). A modified ground-motion attenuation relationship for southern California that accounts for detailed site classification and a basin-depth effect. In *Bulletin of the Seismological Society of America, 90*(6). http://pubs.er.usgs.gov/publication/70022254

Frankel, A., & Vidale, J. (1992). A three-dimensional simulation of seismic waves in the Santa Clara Valley, California, from a Loma Prieta aftershock. *Bulletin of the Seismological Society of America*, *82*(5), 2045–2074.

Galetzka, J., Melgar, D., Genrich, J. F., Geng, J., Owen, S., Lindsey, E. O., Xu, X., Bock, Y., Avouac, J.-P., Adhikari, L. B., Upreti, B. N., Pratt-Sitaula, B., Bhattarai, T. N., Sitaula, B. P., Moore, A., Hudnut, K. W., Szeliga, W., Normandeau, J., Fend, M., & Maharjan, N. et al. (2015). Slip pulse and resonance of the Kathmandu basin during the 2015 Gorkha earthquake, Nepal. *Science*, *349*(6252), 1091–1095. doi:10.1126/science.aac6383 PMID:26249228

Graves, R. W., Pitarka, A., & Somerville, P. G. (1998). Ground-motion amplification in the Santa Monica area: Effects of shallow basin-edge structure. *Bulletin of the Seismological Society of America*, *88*(5), 1224–1242.

Ivanovic & Sanja. (n.d.). Characteristics of Site-Specific Amplifiaction Functions Measured In Montenegro. *13th World Conference on Earthquake Engineering,Vancouver, B.C., Canada, August, 2004*, 12.

Jakka, R. S., Hussain, M., & Sharma, M. L. (2015). Effects on amplification of strong ground motion due to deep soils. *Geomechanics and Engineering*, *8*(5), 663–674. doi:10.12989/gae.2015.8.5.663

Jayalakshmi, S., Dhanya, J., Raghukanth, S. T. G., & Mai, P. M. (2019). 3D seismic wave amplification in the Indo-Gangetic basin from spectral element simulations. *Soil Dynamics and Earthquake Engineering*, *129*, 105923. doi:10.1016/j.soildyn.2019.105923

Kaneko, Y., Ito, Y., Chow, B., Wallace, L. M., Tape, C., Grapenthin, R., D'Anastasio, E., Henrys, S., & Hino, R. (2019). Ultra-long Duration of Seismic Ground Motion Arising From a Thick, Low-Velocity Sedimentary Wedge. *Journal of Geophysical Research. Solid Earth*, *124*(10), 10347–10359. doi:10.1029/2019JB017795

Kaneko, Y., Ito, Y., Chow, B., Wallace, L., Tape, C., D'Anastasio, E., Grapenthin, R., & Hino, R. (2018). Extremely long duration of ground motion arising from sedimentary structures above slow slip areas of the Hikurangi subduction zone. *AGU Fall Meeting Abstracts, 53*. https://adsabs.harvard.edu/abs/2018AGUFM.T53C.05K

Karthik Reddy, K. S. K., Somala, S. N., & Tsang, H.-H. (2021). Response of inelastic SDOF systems subjected to dynamic rupture simulations involving directivity and fling step. *Soil Dynamics and Earthquake Engineering*, *151*, 106992. doi:10.1016/j.soildyn.2021.106992

Kawase, H. (1996). The Cause of the Damage Belt in Kobe: "The Basin-Edge Effect," Constructive Interference of the Direct S-Wave with the Basin-Induced Diffracted/Rayleigh Waves. *Seismological Research Letters*, *67*(5), 25–34. doi:10.1785/gssrl.67.5.25

Knopoff, L., & Ni, X. X. (2001). Numerical instability at the edge of a dynamic fracture. *Geophysical Journal International*, *147*(3), 1–6. doi:10.1046/j.1365-246x.2001.01567.x

Kramer, S. L. (1996). *Geotechnical Earthquake Engineering*. Pearson Education India.

Kumar, A., Anbazhagan, P., & Sitharam, T. G. (2013). Liquefaction Hazard Mapping of Lucknow: A Part of Indo-Gangetic Basin (IGB). [IJGEE]. *International Journal of Geotechnical Earthquake Engineering*, *4*(1), 17–41. doi:10.4018/jgee.2013010102

Lee, C., Chan, Y.-C., Komatitsch, D., Huang, B.-S., & Tromp, J. (2009). Effects of Realistic Surface Topography on Seismic Ground Motion in the Yangminshan Region of Taiwan Based Upon the Spectral-Element Method and LiDAR DTMEffects of Realistic Surface Topography on Seismic Ground Motion in the Yangminshan Region of Taiwan. *Bulletin of the Seismological Society of America*, *99*(2A), 681–693. doi:10.1785/0120080264

Lee, C., Chen, H.-W., & Huang, B.-S. (2008). Simulations of Strong Ground Motion and 3D Amplification Effect in the Taipei Basin by Using a Composite Grid Finite-Difference Method. *Bulletin of the Seismological Society of America*, *98*(3), 1229–1242. doi:10.1785/0120060098

Lee, Y., & Anderson, J. G. (2000). Potential for Improving Ground-Motion Relations in Southern California by Incorporating Various Site Parameters. *Bulletin of the Seismological Society of America*, *90*(6B), S170–S186. doi:10.1785/0120000509

Liu, Z., Liang, J., Huang, Y., & Liu, L. (2016). IBIEM modelling of the amplification of seismic waves by a three-dimensional layered alluvial basin. *Geophysical Journal International*, *204*(2), 999–1023. doi:10.1093/gji/ggv473

Marafi, N., Eberhard, M., Berman, J., Wirth, E., & Frankel, A. (2017). Effects of Deep Basins on Structural Collapse during Large Subduction Earthquakes. *Earthquake Spectra*, *33*(3), 963–997. Advance online publication. doi:10.1193/071916eqs114m

Mascandola, C., Massa, M., Barani, S., Lovati, S., & Santulin, M. (2017). Long-Period Amplification in Deep Alluvial Basins and Consequences for Site-Specific Probabilistic Seismic-Hazard Analysis: An Example from the Po Plain (Northern Italy). *Bulletin of the Seismological Society of America*, *107*(2), 770–786. doi:10.1785/0120160166

Narayan, J. P. (2005). Study of Basin-edge Effects on the Ground Motion Characteristics Using 2.5-D Modelling. *Pure and Applied Geophysics*, *162*(2), 273–289. doi:10.1007/s00024-004-2600-8

Niu, Y., & Dravinski, M. (2003). Direct 3D BEM for scattering of elastic waves in a homogenous anisotropic half-space. *Wave Motion*, *38*(2), 165–175. doi:10.1016/S0165-2125(03)00042-8

Nozu, A., Nagao, T., & Yamada, M. (2006). *Simulation of Strong Ground Motions Based on Site- Specific Amplification and Phase Characteristics*.

Parla, R., Shanmugasundaram, B., & Somala, S. N. (2022). Basin Effects on the Seismic Fragility of Steel Moment Resisting Frames Structures: Impedance Ratio, Depth, and Width of Basin. *International Journal of Structural Stability and Dynamics*, *2250108*, 2250108. doi:10.1142/S0219455422501085

Parla, R., & Somala, S. N. (2022). Seismic ground motion amplification in a 3D sedimentary basin: The effect of source mechanism on amplification of ground motion intensity measures in sedimentary basin. *Journal of Earthquake and Tsunami*, S1793431122500087. doi:10.1142/S1793431122500087

Paudyal, Y. R., Yatabe, R., Bhandary, N. P., & Dahal, R. K. (2012). A study of local amplification effect of soil layers on ground motion in the Kathmandu Valley using microtremor analysis. *Earthquake Engineering and Engineering Vibration*, *11*(2), 257–268. doi:10.1007/s11803-012-0115-3

Rial, J. A., Saltzman, N. G., & Ling, H. (1992). Earthquake-Induced Resonance in Sedimentary Basins. [JSTOR.]. *American Scientist*, *80*(6), 566–578.

Saha, S., Karthik Reddy, K. S. K., & Somala, S. N. (2022). Seismic assessment of steel frame subjected to simulated directivity earthquakes: The unilaterality of fault normal component at various rupture distances. *Journal of Building Engineering*, *47*, 103880. doi:10.1016/j.jobe.2021.103880

Semblat, D., Duval, A. M., & Dangla, P. (2002). Seismic site effects in a deep alluvial basin: Numerical analysis by the boundary element method. *Computers and Geotechnics*, *29*(7), 573–585. doi:10.1016/S0266-352X(02)00017-4

Semblat, K., Kham, M., Parara, E., Bard, P. Y., Pitilakis, K., Makra, K., & Raptakis, D. (2005). Seismic wave amplification: Basin geometry vs soil layering. *Soil Dynamics and Earthquake Engineering*, *25*(7), 529–538. doi:10.1016/j.soildyn.2004.11.003

Semblat, P. R., & Duval, A. M. (2011). Simplified vibratory characterization of alluvial basins. *ArXiv:1108.3403 [Physics]*. https://arxiv.org/abs/1108.3403

Semblat, Parara, E., Kham, M., Bard, P.Y., Pitilakis, K., Makra, K., & Raptakis, D. (2004). *Site Effects: Basin Geometry vs Soil Layering*.

Sharma, B., Chingtham, P., Sharma, V., Kumar, V., Mandal, H. S., & Mishra, O. P. (2017). Characteristic ground motions of the 25th April 2015 Nepal earthquake (Mw 7.9) and its implications for the structural design codes for the border areas of India to Nepal. *Journal of Asian Earth Sciences*, *133*, 12–23. doi:10.1016/j.jseaes.2016.07.021

Sitharam, T. G., & Vipin, K. S. (2010). Evaluation of Peak Ground Acceleration and Response Spectra Considering the Local Site Effects: A Probabilistic Logic Tree Approach. *International Journal of Geotechnical Earthquake Engineering*, *1*(1), 25–41. doi:10.4018/jgee.2010090802

Somala, S. N., Parla, R., & Mangalathu, S. (2022). Basin effects on tall bridges in Seattle from M9 Cascadia scenarios. *Engineering Structures*, *260*, 114252. doi:10.1016/j.engstruct.2022.114252

Steidl, J. H. (2000). Site Response in Southern California for Probabilistic Seismic Hazard Analysis. *Bulletin of the Seismological Society of America*, *90*(6B), S149–S169. doi:10.1785/0120000504

Stephenson, W. J., Williams, R., Odum, J., & Worley, D. (2000). High-resolution seismic reflection surveys and modeling across an area of high damage from the 1994 Northridge earthquake, Sherman Oaks, California. *Bulletin of the Seismological Society of America*, *90*(3), 643–654. doi:10.1785/0119990112

Veggalam, S., Karthik Reddy, K. S. K., & Somala, S. N. (2021). Collapse fragility due to near-field directivity ground motions: Influence of component, rupture distance, hypocenter location. *Structures*, *34*, 3684–3702. doi:10.1016/j.istruc.2021.09.096

Weatherill, G., Kotha, S. R., & Cotton, F. (2020). Re-thinking site amplification in regional seismic risk assessment. *Earthquake Spectra*, *36*(1, suppl), 274–297. doi:10.1177/8755293019899956

Wei, S., Chen, M., Wang, X., Graves, R., Lindsey, E., Wang, T., Karakaş, Ç., & Helmberger, D. (2018). The 2015 Gorkha (Nepal) earthquake sequence: I. Source modeling and deterministic 3D ground shaking. *Tectonophysics*, *722*, 447–461. doi:10.1016/j.tecto.2017.11.024

Whitney, R., & Agrawal, A. K. (2017). Ground Motion Characteristics of the 2015 Gorkha, Nepal, Earthquake and Its Effects on a Prototype Unreinforced Masonry Building. *Journal of Structural Engineering*, *143*(4), 04016220. doi:10.1061/(ASCE)ST.1943-541X.0001717

Wirth, E. A., Vidale, J. E., Frankel, A. D., Pratt, T. L., Marafi, N. A., Thompson, M., & Stephenson, W. J. (2019). Source-Dependent Amplification of Earthquake Ground Motions in Deep Sedimentary Basins. *Geophysical Research Letters*, *46*(12), 6443–6450. doi:10.1029/2019GL082474